Ppm-level Cu dopant on ultrathin Pd nanosheets/TiO$_2$ for highly enhanced photocatalytic alcoholysis of epoxides

Meilin Duan [a], Canyu Hu [a], Delong Duan [a], Ruitian Chen [a], Chengming Wang [a], Di Wu [a],
Tong Xia [a], Hengjie Liu [a], Yitao Dai [a,b,**], Ran Long [a,*], Li Song [a], Yujie Xiong [a,c,**]

[a] School of Chemistry and Materials Science, Frontiers Science Center for Planetary Exploration and Emerging Technologies, and National Synchrotron Radiation Laboratory, University of Science and Technology of China, Hefei, Anhui, 230026, China
[b] Suzhou Institute for Advanced Research, University of Science and Technology of China, Suzhou, Jiangsu, 215000, China
[c] Institute of Energy, Hefei Comprehensive National Science Center, 350 Shushanhu Rd., Hefei, Anhui 230031, China

ARTICLE INFO

ABSTRACT

Photocatalysis provides a new avenue for organic synthesis, to which catalyst design at atomic level holds the key. Herein, the first case of ppm-level (39 ppm) Cu dopant based photocatalyst has been successfully constructed as Cu$_1$Pd$_{200}$/TiO$_2$, in which Cu element dopes ultrathin Pd nanosheets (thickness of 2 nm) with atomic dispersion using TiO$_2$ as the semiconductor host. The alcoholysis of styrene oxide, as a model reaction, can produce valuable β-alkoxy alcohols, conventionally requiring corrosive strong acids or harsh reaction conditions. The presence of ppm-level Cu atoms in Cu$_1$Pd$_{200}$/TiO$_2$ can boost alcoholysis with a quite high reaction rate of 176 mmol·g^{-1}·h^{-1} at room temperature under light illumination (100 mW·cm^2), which is 6 times and 17 times higher than Pd/TiO$_2$ and bare TiO$_2$, respectively. Moreover, the Cu-doped photocatalyst presents excellent stability without deactivation after ten cycles. Based on X-ray photoelectron spectroscopy, infrared spectroscopy and control experiments, this unexpected photocatalytic behavior mainly origins from the electron transfer effect and unique chemisorption of epoxides owing to Cu dopant.

1. Introduction

β-alkoxy alcohols, serving as the precursors for the preparation of immunosuppressive or anti-tumoral medicines, are usually synthesized via the nucleophilic addition of alcohols to epoxides [1–4]. At present, the employment of corrosive supported strong acids (*e.g.*, triflic acid-functionalized silica[5]) or solid acids (*e.g.*, HTiNbO$_5$ [6]) are the most efficient approach to drive alcoholysis of epoxides. Unfortunately, these heterogeneous catalyst systems involving strong acids could corrode the reaction equipment or leach the loaded acids during catalytic processes [5,7]. Besides, they always present ultra-high sensitivity to the external environment, which can be easily poisoned by a tiny number of basic molecules [8]. In contrast, several strong acid-free catalysts (*e.g.*, metal-organic framework Zr-MOF [9] and UiO-66;[10] supported iron complex[11]) have been successfully developed. They usually require external heating with a long reaction time to achieve full conversion (e.g., 24 h for 0.8 mmol styrene oxide with methanol at 55 °C

[9]). Especially, the grafting of metal complex on mesoporous silica even failed to realize the alcoholysis when butanol was used as alcohol candidate, presenting the poor yield of 9% after 144 h [11]. Moreover, MOF-based catalysts can show a wider scope for various epoxides and alcohols, even though the deactivation of MOF-based catalysts was observed due to the poisoning from reaction products [10]. Therefore, a heterogeneous catalytic system without the involvement of strong acids needs to be fabricated with high efficiency and stability.

Recently, photocatalytic organic transformation is emerging as a promising synthetic protocol with mild reaction conditions (e.g., room temperature and ambient pressure) and different reaction pathways in comparison with thermal catalytic counterparts [12–14]. As far as we know, for photocatalytic ring-opening reactions of epoxides, only two cases have been reported [15,16]. In the first case, carbon quantum dots functionalized with -SO$_3$H groups, prepared through the reflux of concentrated sulfuric acid, were reported in 2015 to drive the ring-opening of styrene oxide with methanol under visible light

irradiation [15]. However, the nanocarbon materials presented almost the same activity in dark. Consequently, they probably work as the host of strong acid groups, showing a similar catalytic mechanism when compared with other reported sulfated catalysts [8,17]. The other recent study explored bismuth-based halide perovskite ($Cs_3Bi_2Br_9$) as photocatalyst in 2019, which can successfully drive the alcoholysis of various epoxides [16]. The apparent quantum efficiencies of the $Cs_3Bi_2Br_9$ photocatalytic system for epoxide alcoholysis match well with the light absorption profile, proving light energy as the driving force for alcoholysis. As other photocatalytic redox systems behave [14], this novel halide perovskite-based photocatalyst presents the common problems as well, which points to the poor capacity of reactant amount and low reaction rate (0.1 mmol styrene oxide and 1.3 mmol·g^{-1}·h^{-1} in this study).

It is well known that the modification of metal nanoparticles with another metal species has been considered as one powerful method to reconstruct the electronic structures of metal nanoparticles. This approach can lower the activation energies of reactants (e.g., H_2) and tune their adsorption for selective reactions [18–22]. For example, the Pt-Cu nanoalloy can present different hydrogenation behavior due to H_2 activation and spillover in comparison with the pure Pt or Cu case. Thus, the Pt-Cu alloy can demonstrate high activity and selectivity for hydrogenation of butadiene to butene [21]. More interestingly, the Xiong group has fabricated Pd_7Cu_1 nanoparticles for photocatalytic reduction of CO_2 to CH_4 with high selectivity (up to 96% for methane production). The paired Cu-Pd sites with the elevated d-band center of Cu atoms can promote CO_2 activation and suppress H_2 evolution [22]. However, in terms of the amount from added metal species, quite limited studies tell people whether the ppm-level addition of metal atoms (< 100 ppm) can make a big difference in the final catalytic performance [21,23], especially in the field of heterogeneous photocatalysis.

Herein, based on the fact that Cu species can activate epoxide molecules through coordination [24] and Pd/TiO_2 enables alcohol dissociation as a photocatalyst [25], we propose that the atomic dispersion of Cu dopant on Pd/TiO_2 may boost the photocatalytic alcoholysis of epoxides. Therefore, a photocatalyst with ppm-level Cu dopant (calculated by weight) anchored onto the surface of Pd nanosheets has been established, using TiO_2 as the semiconductor host. To the best of our knowledge, this is the first case of ppm-level Cu dopant based photocatalyst. By using the alcoholysis of styrene oxide with methanol as the model reaction, the photocatalytic activities of as-prepared photocatalysts (Cu doped Pd/TiO_2, Pd/TiO_2 and bare TiO_2) were investigated after the thorough material characterizations such as electron microscopy, UV-Vis spectroscopy, X-ray diffraction and X-ray photoelectron spectroscopy. To gain more insights into photocatalytic mechanisms, control experiments, infrared spectroscopy and chemisorption analysis were elaborately designed. The characterization data of photocatalysts, photocatalytic reaction performance and proposed reaction mechanism could offer a deep understanding of the structure-activity relationship for the ppm-level Cu dopant based photocatalyst, which may promote its further application in other catalytic processes.

2. Experimental

2.1. Photocatalyst preparation

For the synthesis of TiO_2 as the semiconductor host [26], 10 mL Ti$(OBu)_4$ and 1.2 mL hydrofluoric acid were added to a 50 mL Teflon autoclave, which was kept at 180 ℃ for 24 h. After being cooled to room temperature, the supernatant yellow liquid was decanted. The solid sample was separated by centrifuging at 6000 rpm for 5 min and washed with deionized water and ethanol at least four times. Finally, the TiO_2 powder was obtained after drying at 60 ℃ in a vacuum oven for 12 h.

The ultrathin Pd nanosheets were prepared by a wet-chemical process according to the reported literature [27,28]. In detail, 170 mg citric acid, 30 mg polyvinylpyrrolidone (PVP, molecular weight of 29,000), 60 mg hexadecyl trimethyl ammonium bromide (CTAB), and 16 mg Pd

$(acac)_2$ were dissolved in 10 mL N, N-dimethylformamide (DMF) in a 50 mL flask, in which an orange-red solution was formed. After magnetically stirring for 1 h, 100 mg W$(CO)_6$ was added into the solution under N_2 atmosphere, which was heated to 80 ℃ for 1 h. Later, the flask was taken out from the oil bath and cooled down to room temperature. To obtain the Pd sample, 30 mL acetone was added into the flask for centrifugation (8000 rpm for 5 min). After the washing step with 40 mL acetone and 5 mL ethanol three times (10,000 rpm for 5 min), the sediment was dispersed in 8 mL ethanol for the following usage (containing 5.6 mg Pd nanosheets).

The Cu_1Pd_{200} nanosheets were synthesized by use of the same method except for the extra addition of 520 μL DMF solution with 16 mM $CuCl_2$ to the above orange-red solution containing Pd precursors.

For comparison, Cu nanoparticles (Cu_{NP}) were deposited on Pd nanosheets by use of a similar synthesis procedure except that the following parameters were changed: 16 mM $CuCl_2$ based DMF solution (3.28 mL) and 150 mg W$(CO)_6$ were added and the heating temperature was enhanced to 120 °C.

For the synthesis of Pd/TiO_2, Cu_1Pd_{200}/TiO_2 (i.e., Cu dopant based photocatalyst), or Cu_{NP}/Pd/TiO_2 (i.e., Cu NP based photocatalyst), 50 mg as-prepared TiO_2 host was dispersed in a flask with 20 mL deionized water under magnetically stirring. Then 1 mL ethanol solution containing Pd, Cu_1Pd_{200}, or Cu_{NP}/Pd nanosheets (containing 0.7 mg Pd, Cu_1Pd_{200}, or Cu_{NP}/Pd) was added to the above TiO_2 suspension. Subsequently, the whole gray mixture experienced ultrasonic treatment for another 10 min, which was later heated at 80 ℃ in an oil bath under magnetically stirring for 1 h. Afterward, the Pd/TiO_2, Cu_1Pd_{200}/TiO_2, or Cu_{NP}/Pd/TiO_2 wet sample was separated by centrifugation (6000 rpm for 5 min) and washed with deionized water twice. Finally, the Pd/TiO_2, Cu_1Pd_{200}/TiO_2, or Cu_{NP}/Pd/TiO_2 powder was obtained after drying at 60 ℃ in a vacuum oven for 12 h.

2.2. Characterizations

The transmission electron microscopy (TEM) images were measured on a HITACHI HT7700 system with an electron accelerating voltage of 100 kV, and high-resolution transmission electron microscopy (HRTEM) images and energy-dispersive spectroscopy (EDS) mapping were measured on a JEOL JEM-2100 instrument with an electron accelerating voltage of 200 kV. Powder X-ray diffraction (XRD) patterns were characterized on a Rigaku SmartLab 9 kW rotation anode X-ray diffractometer with graphite monochromated Cu Kα radiation. XRD patterns were scanned over the angular range of 10–80° (2θ) with a step size of 0.02°. X-ray photoelectron spectroscopy (XPS) measurements were performed on an ESCALAB 250Xi XPS system (Thermo Scientific, Udopant) with a monochromatic Al Kα source. All the binding energies were referenced to the C1s peak at 284.6 eV of the surface adventitious carbon. The amount of Cu, Pd, and Ti were determined on an Inductively Coupled Plasma Optic Emission Spectrometer (ICP-OES, Opmita 7300 DV) and Inductively Coupled Plasma Mass Spectrometer (ICP-MS, X Series 2). Extended X-ray absorption spectra (EXAFS) were measured on the BSRF-1W1B in Beijing Synchrotron Radiation Facility. UV–visible near-infrared absorption spectra of solid powders were obtained by use of Shimadzu 3700 with $BaSO_4$ (spectroscopy grade) as a reference. Photoluminescence was analyzed with the powder sample dispersed in acetone (0.07 mg·mL^{-1}) by use of a fluorescence spectrophotometer (HITACHI F-4600), in which 325 nm was employed for excitation.

The infrared spectra (IR) were performed on a Fourier Transform Infrared Spectrometer (Nicolet 8700). Firstly, the samples were mixed with KBr (≥99.0%, Sinopharm Chemical Reagent Co., Ltd.) power (2.5 mg Cu_1Pd_{200}/TiO_2, Pd/TiO_2 or TiO_2 with 400 mg KBr; 0.2 mg Cu_1Pd_{200} or Pd with 400 mg KBr). The mixture was ground for 10 min then pressed at 20 MPa to form a flake sample for the IR test. Before collecting the IR spectra of photocatalysts adsorbed with styrene oxide, the flake samples were placed in a 40 mL airtight glass tube containing 30 μL of styrene oxide for 6 h. The IR spectra were scanned over the wavenumber

range of 4000–400 cm^{-1} with a step size of 0.4821 cm^{-1}. For the heat treatment of the flake samples with probe molecules adsorbed, the samples were heated in a tubular oven with an Ar flow (10 mL·min^{-1}) at a certain temperature (25, 80, or 200 °C). The in-situ diffuse reflectance infrared Fourier-transform spectroscopy (DRIFTS) measurements were performed on a Bruker IFS 66 v Fourier-transform spectrometer equipped with a Harrick diffuse reflectance accessory at the Infrared Spectroscopy and Microspectroscopy Endstation (BL01B) in National Synchrotron Radiation Laboratory (NSRL) in Hefei, China. Each spectrum was recorded by averaging 265 scans at a resolution of 4 cm^{-1}. The background with samples was collected after purging argon gas flow (20 mL·min^{-1}) into the sample chamber for 15 min. Subsequently, methanol was carried into the sample chamber by argon gas flow for 20 min. After purging the chamber with argon flow for another 15 min to remove the physisorbed methanol, the IR spectrum was collected. The tests of H$_2$ temperature-programmed desorption (TPD) were conducted on a chemisorption analyzer (AutoChem II) coupled with a mass spectrometer (MS, OmniStar GSD, Pfeiffer). The detailed H$_2$-TPD procedure is as follows: 50 mg sample was loaded into a U-type quartz tube and pretreated in a 10% H$_2$/He flow of 20 mL·min^{-1} at 200 °C for 30 min. After cooling, desorption profiles were obtained by passing a flow of He (50 mL·min^{-1}) through the sample, the outlet of which was monitored by the coupled MS. Meanwhile, the temperature was controlled to increase gradually from 100° to 230°C at a rate of 10 °C min^{-1}.

2.3. Photocatalytic evaluation

The photocatalytic reactions were carried out in a sealed quartz tube at room temperature with a 300 W Xe lamp as the light source (Perfect Light, PLS-SXE300). Typically, 5 mg photocatalyst was dispersed in 2 mL methanol with 100 mg (0.88 mmol) styrene oxide. After the replacement of the gas atmosphere in a quartz tube with Ar, the reaction suspension was illuminated under magnetically stirring for a certain time. The light intensity was set at 100 mW·cm^2, which was measured by an optical power meter (FZ-A, Beijing Shida Photoelectric Technology Co., Ltd). For the visible light irradiation, a 420 nm filter was used to cut off the light with a wavelength shorter than 420 nm. For the UV irradiation case, a UV reflector was located at 45 degrees in front of the lamp. After irradiation, the reaction suspension was centrifuged with the liquid phase quantified by gas chromatography (GC) systems with J&W HP-5 ms GC Column (30 m * 0.25 mm*0.25 μm, 7-inch cage). For qualitative analysis, Agilent mass spectrometry (MS) 5975 C inert XL MSD with Triple-Axis detector has been employed. The yield referred to the GC yield, calculated based on the conversion of styrene oxide and the selectivity of the desired product. The conversion was the ratio of consumed styrene oxide to the added styrene oxide before reaction, while the selectivity of 2-methoxy-2-phenylethanol was calculated by the molar percentage of 2-methoxy-2-phenylethanol in total products. Phenylethanol was added after reaction as the external standard for quantitative analysis. Additionally, for the photocatalytic H$_2$ evolution tests, all the procedures are the same as the above alcoholysis tests except that 5 mg photocatalyst was added to 5 mL methanol. After the reaction, the gas phase in the quartz tube was sampled and analyzed by GC for quantification. The cycling tests were carried out with the same light intensity and amount of styrene oxide for each cycle. After reaction, the mixture was centrifuged to separate the heterogeneous photocatalyst. After washed with methanol for three times, the photocatalyst was suspended in methanol solution with styrene oxide for the next cycling test.

3. Result and discussion

3.1. Characterizations of Cu dopant based photocatalyst

After the loading of Cu$_1$Pd$_{200}$ on a semiconductor host of TiO$_2$ via a simple mixing process, the Cu-doped photocatalyst can be fabricated as

shown in Scheme 1. Based on the TEM analysis shown in Fig. 1(a), the as-prepared TiO$_2$ host presents a platelet-like morphology with the rectangular contour, whose thickness is ~6 nm and slide length is ~40 nm. In contrast, as-synthesized Pd nanosheets display a hexagonal outline with an average basal plane size of ~24 nm and the thickness as thin as 2 nm (Fig. 1(b) and Fig. S1). It is should be mentioned that a small number of Pd nanocrystals with rhombus shape appear as dark domains, which also matches with the reported case [28]. For the sample of Cu$_1$Pd$_{200}$ nanosheets shown in Fig. 1(c), the incorporation of Cu atoms into Pd nanosheets demonstrates no changes in morphology. XRD profiles of Cu$_1$Pd$_{200}$ and Pd nanosheets are exactly the same as shown in Fig. S2, which verify the presence of Pd with a face-centered cubic (fcc) structure. Moreover, the HRTEM image in Fig. 1(d) of Cu$_1$Pd$_{200}$ nanosheets indicates the lattice fringes with an interplanar spacing of 2.3 Å [27,28], corresponding well to the [111] planes of fcc Pd. This may suggest that Cu atoms are mainly located on the surface of the Pd nanosheet, not inside its crystal structure [29]. To verify the successful introduction of the Cu element, an analysis of EDS mapping has been conducted for the Cu$_1$Pd$_{200}$ sample. As demonstrated in Fig. 1(e-h), the distribution of Pd and Cu elements overlaps well with the scanning TEM (STEM) image, illustrating the high dispersion of Cu on Pd nanosheets. Furthermore, the loading of Cu$_1$Pd$_{200}$ nanosheets can be clearly observed in the TEM image of the Cu$_1$Pd$_{200}$/TiO$_2$ sample, which is marked by the red circles in Fig. (i). These darker domains with ~2 nm in thickness correspond to the side-view of Cu$_1$Pd$_{200}$ nanosheets (thickness of 2 nm) attached on TiO$_2$ surface. Besides, Pd/TiO$_2$ sample without Cu atoms presents the same morphology with Cu$_1$Pd$_{200}$/TiO$_2$ (Fig. S3).

To confirm the content of metal elements, ICP-MS and ICP-OES were employed to analyze supported samples (Table S1). For the sample of Cu$_1$Pd$_{200}$/TiO$_2$, the atomic ratio of Cu:Pd:Ti equals 1:200:20000, which corresponds to an ultra-low loading of 39 ppm Cu atoms in weight and total loading of 1.32 wt% from Cu$_1$Pd$_{200}$ nanosheets. Similarly, the atomic ratio of Pd:Ti for the Pd/TiO$_2$ sample is identified as 1:97, implying that the loading of Pd nanosheets reaches 1.36 wt%. Apparently, almost all the Pd or Cu$_1$Pd$_{200}$ nanosheets (0.7 mg) are successfully adsorbed onto the surface of TiO$_2$ (50 mg) during the catalyst synthesis. Due to the low loading of Pd nanosheets or Cu$_1$Pd$_{200}$ nanosheets (~1.3 wt%), X-ray diffraction (XRD) data shown in Fig. 2(a) only presents the anatase phase of the TiO$_2$ host (JCPDS No. 21–1271). Besides, the UV-Vis absorption profiles of both supported samples in Fig. 2(c) also only show the main light absorption in the UV region due to the TiO$_2$ host. Based on their Tauc plots (Fig. S4) [30,31], the optical bandgap values of both Cu$_1$Pd$_{200}$/TiO$_2$ and Pd/TiO$_2$ amount to 3.22 eV, which is exactly the same with bare anatase TiO$_2$ [32]. It should be noted that both Cu$_1$Pd$_{200}$ and Pd nanosheets exhibit a quite weak absorption band starting from 600 nm (Fig. S5), which is contributed to the surface plasmon resonance of Pd metals with ultrathin nanostructures as reported [33].

To unlock the structural information of Cu and Pd atoms in the ultrathin nanosheets, X-ray absorption fine structure (XAFS) spectroscopy via synchrotron radiation was conducted on the Cu$_1$Pd$_{200}$/TiO$_2$ sample. Fig. S6 showed the Pd K-edge X-ray absorption near-edge structure (XANES) spectra in reference to standard Pd foil, suggesting the main oxidation state of Pd in Cu$_1$Pd$_{200}$ nanosheets to be metallic. After a Fourier-transform, the Pd K-edge EXAFS spectra are evolved in Fig. 2(c). To acquire the local bonding information of Pd, the metal-metal bond lengths and metal coordination numbers (CN) had been extracted through fitting the EXAFS curve. As shown in Table S2, compared with the characteristic Pd-Pd bond in Pd foil (2.75 Å), the main peak of the Pd K-edge profile in the Cu$_1$Pd$_{200}$/TiO$_2$ sample is slightly shifted to a longer bond length (2.78 Å). This minor shift can be originated from the slight lattice expansion of Pd because of the ultrathin nanostructure [34]. The Pd K-edge spectrum indicates the average coordination number of Pd in Cu$_1$Pd$_{200}$/TiO$_2$ to be 8.3, suggesting the unsaturated coordination of Pd in contrast to the Pd foil with a CN of 12. This unsaturated coordination
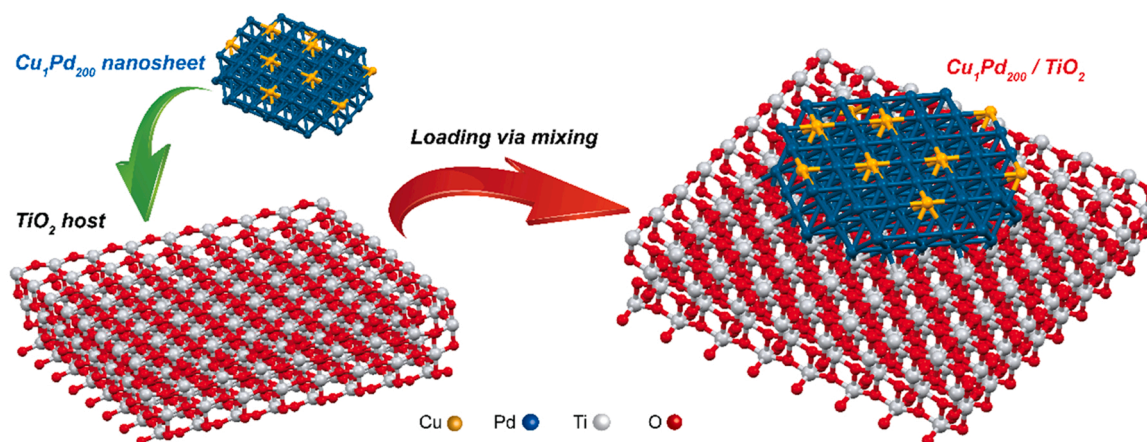
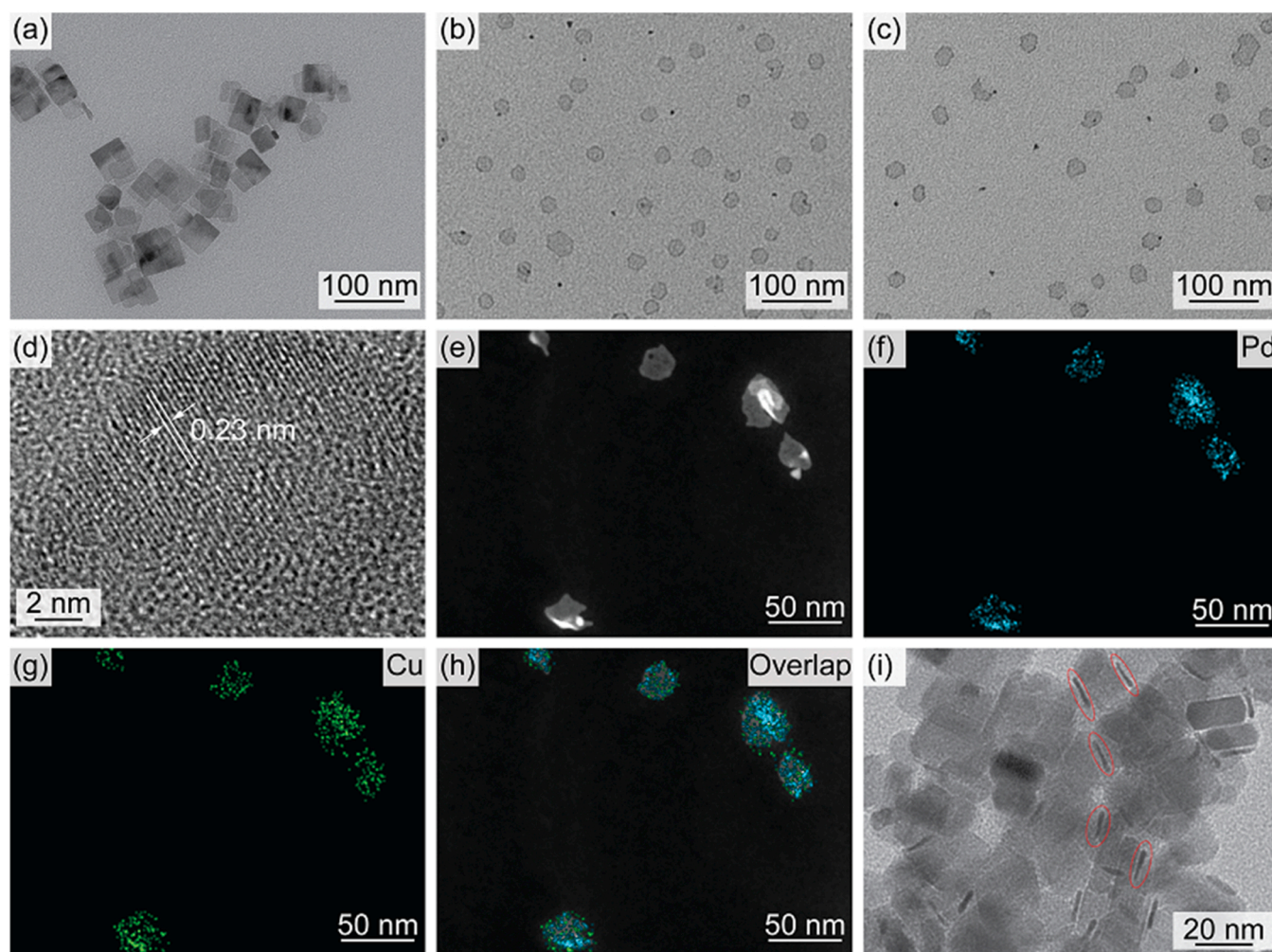**Scheme 1.** Schematic illustration of loading Cu_1Pd_{200} nanosheets on the surface of TiO_2 host.

Fig. 1. TEM images of (a) TiO_2, (b) Pd nanosheets and (c) Cu_1Pd_{200} nanosheets; (d) HRTEM and (e) STEM images of Cu_1Pd_{200} nanosheets; (f-g) EDS elemental mapping profiles of Cu_1Pd_{200} nanosheets with Cu (green) and Pd (blue) distribution; (h) overlap image of STEM and elemental mapping data; (i) TEM image of Cu_1Pd_{200}/TiO_2 sample with red circles labeling the loading of Cu_1Pd_{200} nanosheets. (For interpretation of the references to colour in this figure, the reader is referred to the web version of this article.)

is consistent with the ultrathin structure of Pd nanosheets with a high surface ratio (~25%). The high surface atomic ratio could also facilitate the surface Pd to be doped by Cu atoms. Regarding the oxidation state of

Cu atoms in Cu_1Pd_{200} nanosheets, it can be revealed by the Cu K-edge XANES spectra in reference to standard Cu foil and Cu_2O (Fig. S7). The pre-edge peak in Cu_1Pd_{200} nanosheets locates at 8994.0 eV, which is
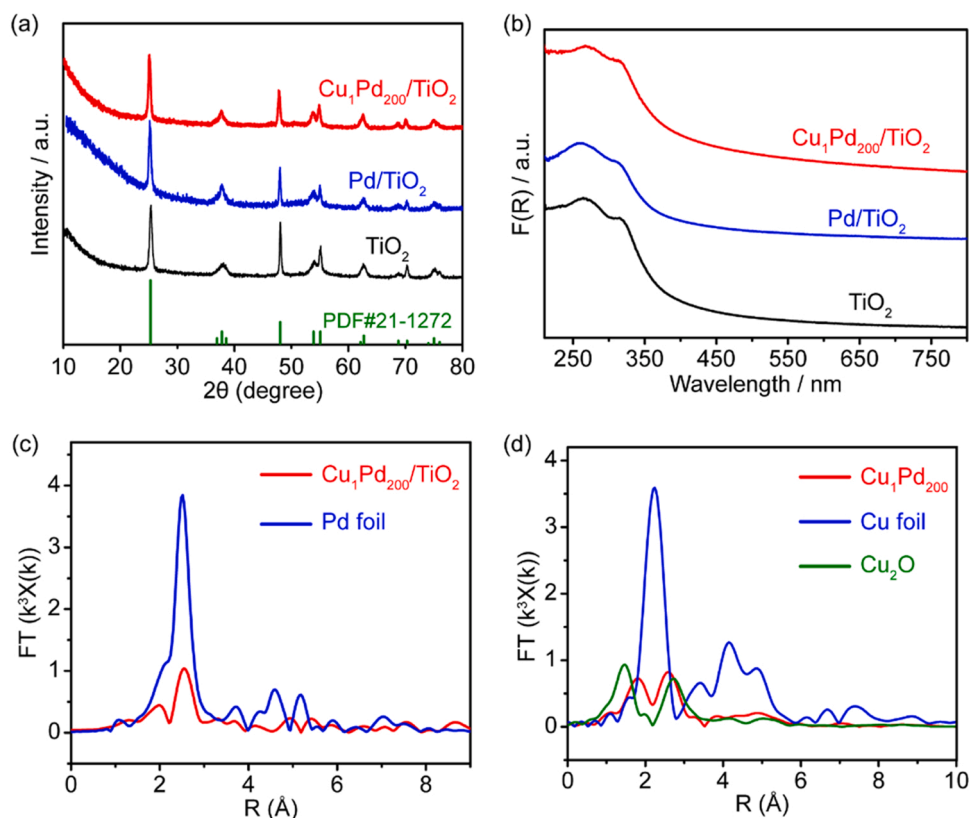
Fig. 2. (a) XRD profiles and (b) UV-Vis absorption spectra of Cu_1Pd_{200}/TiO_2, Pd/TiO_2, and TiO_2 samples; k^3-weighted Fourier-transform EXAFS spectra of (c) Cu_1Pd_{200}/TiO_2 in reference to Pd foil and (d) Cu_1Pd_{200} with Cu foil and Cu_2O as references.

slightly higher than that of Cu foil (8993.5 eV) and much lower than that of Cu_2O (8995.4 eV). Thus, metallic Cu can be identified as the main state even though minor Cu^+ may exist. For more structural information of Cu atoms in Cu_1Pd_{200} nanosheets, the Cu K-edge EXAFS profile with k^3-weighted Fourier-transform shown in Fig. 2(d) implies that the bond at 2.64 Å can be assigned to Cu-Pd bond based on modeling. Moreover, the Cu-Cu bond at 2.54 Å in Cu foil does not appear in the Cu_1Pd_{200} sample. Therefore, the Cu element dopes Pd nanosheets with a high dispersion up to an atomic level. In addition, as shown in Table S2 the average coordination number of Cu-Pd is calculated to be 5.25, which is much less than that of Cu-Cu in Cu foil or Pd-Pd in Pd foil (CN = 12 for both). This highly unsaturated coordination suggests that the Cu dopant is mainly dispersed on the surface of Pd nanosheets. Moreover, the comparison with EXAFS data from reference Cu_2O indicates the Cu-O

bond (1.84 Å) could be ruled out for Cu dopant in Cu_1Pd_{200} nanosheets. In contrast, the shorter bond from Cu dopant at 2.22 Å may be contributed to the Cu-Cl bond according to the fitting data in Table S2. This Cl species could probably come from the precursor of $CuCl_2$ during catalyst synthesis. Coupling with the Cu K-edge XANES data of Cu_1Pd_{200} nanosheets (Fig. S7), we deduce that only a minor portion of Cu dopant may present as the Cu-Cl state.

The modification of one metal substrate with another metal species is commonly considered as an efficient approach to reconstruct the electronic structures of metals [35]. It can be realized by different protocols such as doping [36,37], alloying [22,38,39] and depoistion [27,40,41]. In our case, the ppm-level Cu atoms on the surface of Pd nanosheets behave as doping. To gain more signals from samples, Cu_1Pd_{200} and Pd nanosheets were used for XPS analysis, since the loading of Cu or Pd is
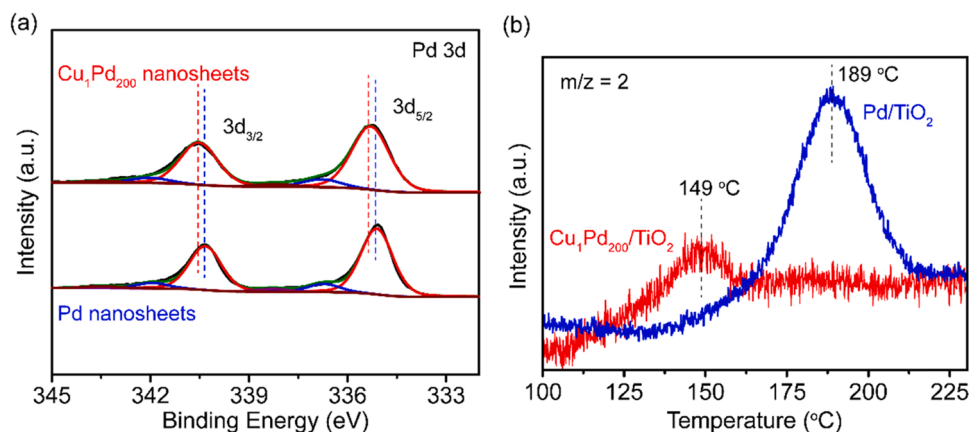

Fig. 3. (a) Pd 3d XPS profiles of Cu_1Pd_{200} nanosheets in comparison with the Pd counterpart. (b) H_2-TPD analysis of Cu_1Pd_{200}/TiO_2 and Pd/TiO_2 samples.

low in both supported photocatalysts. Fortunately, the XPS analysis in Fig. 3(a) clearly demonstrates the influence of Cu dopant on Pd substrates. The binding energies of Pd $3d_{3/2}$ and $3d_{5/2}$ peaks for Cu_1Pd_{200} nanosheets are apparently shifted to higher values (340.6 and 335.3 eV) in comparison with those for Pd nanosheets (340.4 and 335.1 eV). The shifts can be ascribed to the partial electron transfer from Cu atoms to Pd ones because of the lower work function of Cu than Pd (4.65 eV and 5.12 eV for Cu and Pd, respectively). This phenomenon also matches well with the reported cases of Pt-Co [42] and Cu-Pd [43] nanoalloys. For Cu_1Pd_{200} nanosheets, the Pd element mainly exists as the metallic state, which is consistent with the above XAFS analysis as well [44]. However, the identification of the Cu element from XPS analysis failed as expected due to the ultra-low loading of Cu dopant. To further verify the influence of Cu dopant on Pd nanosheets, H_2 has been chosen as a probe molecule via H_2-TPD experiments. Both supported photocatalysts (Cu_1Pd_{200}/TiO_2 and Pd/TiO_2) were pre-treated with 10% H_2/He flow at 200 °C for 30 min before TPD tests. As shown in Fig. 3(b), the H_2 desorption peak of Pd/TiO_2 locates at 189 °C, which matches well with the reported data [45,46]. It indicates the strong interaction between Pd and hydrogen atoms as expected, since Pd could form hydride with hydrogen atoms readily diffused within the crystal lattice of Pd [47,48]. The incorporation of Cu dopant on Pd nanosheets can obviously shift this desorption peak to a lower temperature zone at 149 °C, suggesting lower chemisorption energy of H_2. The shift can be contributed to the electron transfer effect characterized by above XPS analysis. This effect can reconstruct the electronic structure of Pd with a lower d-band center, thus facilitating the liberation of H atoms on Pd as H_2 gas with the

weakened chemisorption [18,19,43]. The much lower amount of H_2 desorbed from Cu_1Pd_{200}/TiO_2 can be well understood when the sample was pre-treated in the H_2 atmosphere at 200 °C, which is quite higher than its desorption temperature.

3.2. Investigation on the photocatalytic alcoholysis of styrene oxide with methanol

The presence of metallic Cu dopant atoms on the surface of Pd nanosheets may activate the C-O bond in the three-member ring of epoxide due to the complexing effect. Therefore, the alcoholysis of styrene oxide with methanol has been systematically investigated as a model reaction. As shown in Fig. 4(a), the ppm-level Cu dopant based photocatalyst (Cu_1Pd_{200}/TiO_2) presents the full yield of 2-methoxy-2-phenylethanol after 60-min light irradiation, corresponding to an ultra-high average reaction rate of 176 mmol·g^{-1}·h^{-1}. This rate is almost two orders of magnitude higher than that of the reported halide perovskite based photocatalytic system (1.33 mmol·g^{-1}·h^{-1}) [16]. Even though other byproducts such as benzaldehyde and phenylacetaldehyde appear as well, their total amount accounts for less than 1%. In contrast, the photocatalyst without Cu dopant (Pd/TiO_2) can convert only 50% styrene oxide after even 180 min with a reaction rate of 29 mmol·g^{-1}·h^{-1}. Bare TiO_2 displays the worst photocatalytic performance with a yield of 17% after 180 min, which relates to a low reaction rate of 10 mmol·g^{-1}·h^{-1}. Furthermore, in the case of the most efficient photocatalyst (Cu_1Pd_{200}/TiO_2), the reaction runs much slower before 30 min, which can be due to activation of reactants and the

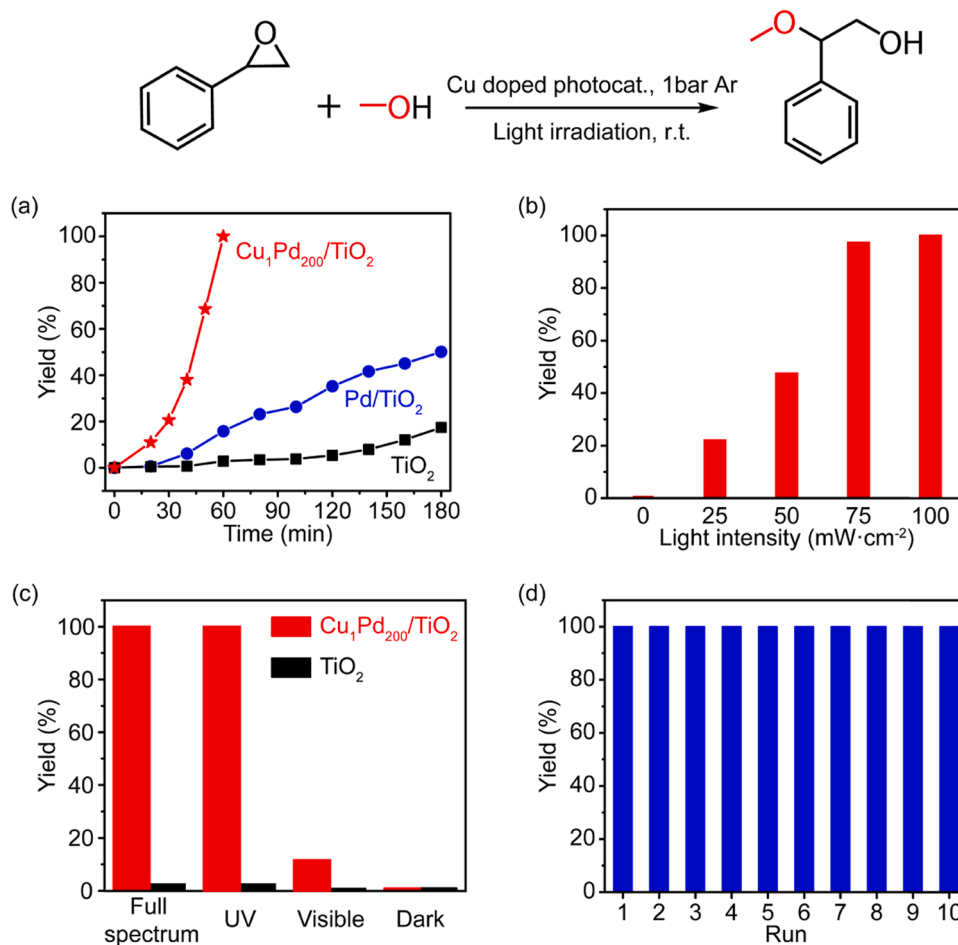**Fig. 4.** (a) Time-dependent alcoholysis of styrene oxides with methanol over Cu_1Pd_{200}/TiO_2, Pd/ TiO_2, and TiO_2 photocatalyst; (b) photocatalytic performance of Cu_1Pd_{200}/TiO_2 for alcoholysis reaction under different light intensity; (c) the influence of different light region in wavelength on the photocatalytic activity of Cu_1Pd_{200}/TiO_2 and bare TiO_2 for alcoholysis reaction; (d) Stability evaluation of Cu_1Pd_{200}/TiO_2 for alcoholysis reaction with 10 cycles.

accumulation of active radical species (such as methoxy radical). Afterward, the styrene oxide is converted in an unexpected linear way with a much higher reaction rate (332 mmol·g^{-1}·h^{-1}). This unusual reaction behavior may originate from the involvement of chain reactions. More interestingly, when Cu nanoparticles (NP) with the size around 4 nm have been deposited on Pd nanosheets (based on TEM and EDS analysis in Fig. S8), the formed Cu$_{NP}$/Pd/TiO$_2$ also presents a higher activity (yield of 43% after 60 min) than Pd/TiO$_2$, further evidencing the promotion effect from the Cu element. However, the activity of Cu dopant based photocatalyst with a reaction rate of 176 mmol·g^{-1}·h^{-1} is quite superior to that of Cu NP counterpart, whose reaction rate is 76 mmol·g^{-1}·h^{-1} and Cu loading is greatly increased to 0.1 wt% based on ICP-OES analysis in Table S1. These big differences in photocatalytic activity and Cu loading obviously demonstrate the tremendous superiority from atomic dispersion of Cu element on the surface, which can not only dramatically promote the reaction performance but also incredibly reduce the Cu loading to a ppm-level.

To clarify the influence from heat, the reaction temperature has been monitored (Fig. S9), reaching 38.2 °C after the illumination with a light intensity of 100 mW·cm^2. Moreover, experiments with different reaction temperatures (from 25 to 80 °C) have been conducted (Fig. S10). Under dark conditions, poor yields of 3.5% and 6.9% are observed at 40 and 80 °C respectively. In comparison, a full yield is achieved under light irradiation at either 25 °C or 80 °C. This big difference indicates that the thermal effect is negligible and photo-excited charges drive the reaction in our photocatalytic system. As expected, the photocatalytic activity gradually increases with the light intensity varying from 25 to 100 mW·cm^2 (Fig. 4(b)), identifying the alcoholysis of epoxides over Cu$_1$Pd$_{200}$/TiO$_2$ as a photon-dependent process.

To further explore the contribution from the plasmonic effect of Pd nanosheets, light with different regions in wavelength has been irradiated (Fig. 4(c)). The case of UV light presents a full yield, which is the same as the case by use of the light with a full spectrum. However, the yield drops remarkably to 11.6% when irradiated under visible light (> 420 nm). Thus, the electrons and holes generated from the TiO$_2$ host are the main charges to drive the alcoholysis of styrene oxide. The photocatalytic activity observed in the case of visible light can be ascribed to the plasmonic photocatalysis from Cu$_1$Pd$_{200}$ nanosheets. Because quite similar photocatalytic activity (the yield of 10.6%) has been obtained when using Cu$_1$Pd$_{200}$ nanosheets as photocatalyst under visible light irradiation, while bare TiO$_2$ shows the negligible yield of 1%. To study the stability of our Cu-doped photocatalyst, Cu$_1$Pd$_{200}$/TiO$_2$ has been evaluated up to 10 cycles. Fortunately, no deactivation has been observed in the stability tests (Fig. 4(d)), demonstrating the full yield of desired β-alkoxy alcohol for each cycle. Moreover, the ppm-level Cu element has been well maintained after the alcoholysis reaction based on ICP analysis of the used photocatalyst (Table S1). The TEM characterizations of the used sample indicate that the loading of Cu$_1$Pd$_{200}$ nanosheets on the TiO$_2$ host is preserved without any change of their nanostructures (Fig. S11). Additionally, XRD analysis also shows the unchanged crystal phase of TiO$_2$ after usage (Fig. S12).

3.3. Mechanistic studies

Overall, extraordinary enhancement in photocatalytic performance has been brought by ppm-level Cu dopant. To provide insights into the photocatalytic mechanism behind this unexpected promotion, we have conducted a series of control experiments and spectroscopy analyses during the adsorption of organic molecules (alcohol and epoxide) on the Cu-doped photocatalyst.

Based on the proposed reaction mechanism from the literature [16], two main reaction steps are involved during the nucleophilic addition in the alcoholysis reaction, including the generation of active methoxy radicals/anions and the activation of epoxides. Firstly, to investigate the activation capability of alcohols, a series of experiments for photocatalytic H$_2$ evolution in methanol have been conducted over different

photocatalysts (Cu$_1$Pd$_{200}$/TiO$_2$, Pd/TiO$_2$, and bare TiO$_2$). As shown in Fig. 5(a), Cu$_1$Pd$_{200}$/TiO$_2$ presents the highest H$_2$ production rate of 15 mmol·g^{-1}·h^{-1}, while Pd/TiO$_2$ produces H$_2$ with a lower rate of 9.5 mmol·g^{-1}·h^{-1}. Almost no activity is observed in the bare TiO$_2$ case as expected due to the serious electron-hole recombination when no noble metal is deposited as a co-catalyst [25]. The promotion from Cu dopant in contrast to the Pd/TiO$_2$ without Cu element can be associated with the electron transfer effect and lower chemisorption of H$_2$, which is well verified by above XPS and H$_2$-TPD tests. Besides, as shown in Fig. S13 photoluminescence analysis demonstrates a lower emission peak (at 403 nm) from Cu$_1$Pd$_{200}$/TiO$_2$ in comparison with Pd/TiO$_2$, suggesting the suppressed radiative recombination in Cu dopant based photocatalyst. Therefore, more charges could be utilized to activate alcohols because of the promoted electron-hole separation. Typically methanol molecules are adsorbed and dissociated to form chemisorbed CH$_3$O species (CH$_3$O$_a$) at surface oxygen vacancy sites (O$_v$) or fourfold-coordinated Ti$_{4c}$ sites under dark on TiO$_2$ surface [49]. After light irradiation, the CH$_3$O$_a$ can be oxidized to produce formaldehyde or methyl formate via photo-generated holes [50]. Meanwhile, H atoms from methanol are cleaved and transferred to the metal surface with electrons, which drive the reduction to generate H$_2$ molecules [49]. The higher activity of H$_2$ evolution on Cu$_1$Pd$_{200}$/TiO$_2$ in methanol implies its stronger ability to activate alcohol molecules, facilitating the following alcoholysis steps. It should be pointed out that during the alcoholysis reaction, almost no H$_2$ was detected. This makes sense when the H$_2$ evolution rate (15 mmol·g^{-1}·h^{-1}) is much lower than that of the alcoholysis reaction (176 mmol·g^{-1}·h^{-1}).

To further explore the activation of methanol on different photocatalysts, in-situ DRIFTS analysis has been performed on the samples with methanol adsorption. As displayed in Fig. 5(b), the C-H bond vibration at 2818 cm^{-1} and 2917 cm^{-1} can be designated to the CH$_3$O$_a$ species, while the absorption peak at 2849 cm^{-1} and 2951 cm^{-1} come from the C-H bond vibration of adsorbed CH$_3$OH species. Notably, the enhancement in the dissociation of methanol to CH$_3$O$_a$ is clearly observed when Cu$_1$Pd$_{200}$ or Pd nanosheets are loaded on TiO$_2$. This probably comes from the strong binding ability of Pd metals to hydrogen, which can accept more H atoms dissociated from the O-H bond of CH$_3$OH. Moreover, the incorporation of Cu dopant on the surface of Pd nanosheets can further promote this dissociation according to IR spectra. We speculate that Cu dopant could offer a unique adsorption site for methoxy species. Since Cu$_1$Pd$_{200}$ nanosheets or Pd nanosheets were dispersed in ethanol after material synthesis, IR characterizations of these samples after the direct heating under different heating temperatures in an inert gas atmosphere can provide useful information regarding alcohol adsorption (Fig. S14). Obviously, after mild heating (at 25 and 80 °C), most of the alcohol molecules leave the surface of Pd nanosheets, presenting almost the same IR absorption as that of the Pd sample with a clean surface after heating at 200 °C (Fig. S14 (a)). In contrast, two main absorption bands belonging to chemisorbed ethanol (1025 and 1096 cm^{-1}) disappear only at 200 °C for Cu$_1$Pd$_{200}$ nanosheets (Fig. S14 (b)), identifying the strong adsorption of alcohols on Cu sites via C-O bonds. Therefore, more active methoxy species can be produced to accelerate the next alcoholysis step over Cu-doped photocatalyst due to its strong adsorption of alcohols. Based on the above results, Cu dopant may demonstrate the unique chemisorption of an epoxide molecule, which presents the C-O bond in a three-member ring as well. After obtaining a clean surface on the Cu$_1$Pd$_{200}$ and Pd nanosheets via heating at 200 °C for 2 h in Ar atmosphere, styrene oxide as another important reactant has been deposited for IR analysis. As shown in Fig. 5(c), the appearance of absorption bands at 698, 758, and 1027 cm^{-1} has been observed on both Cu$_1$Pd$_{200}$ and Pd nanosheets, corresponding to characteristic phenyl C-H bond and ring stretching of styrene oxide [51,52]. This also implies the successful adsorption of styrene oxide on the surface of both nanosheet samples. In comparison with pure styrene oxide and a clean sample of Cu$_1$Pd$_{200}$, a weak absorption peak with the vibrational frequency located at 1092 cm^{-1}
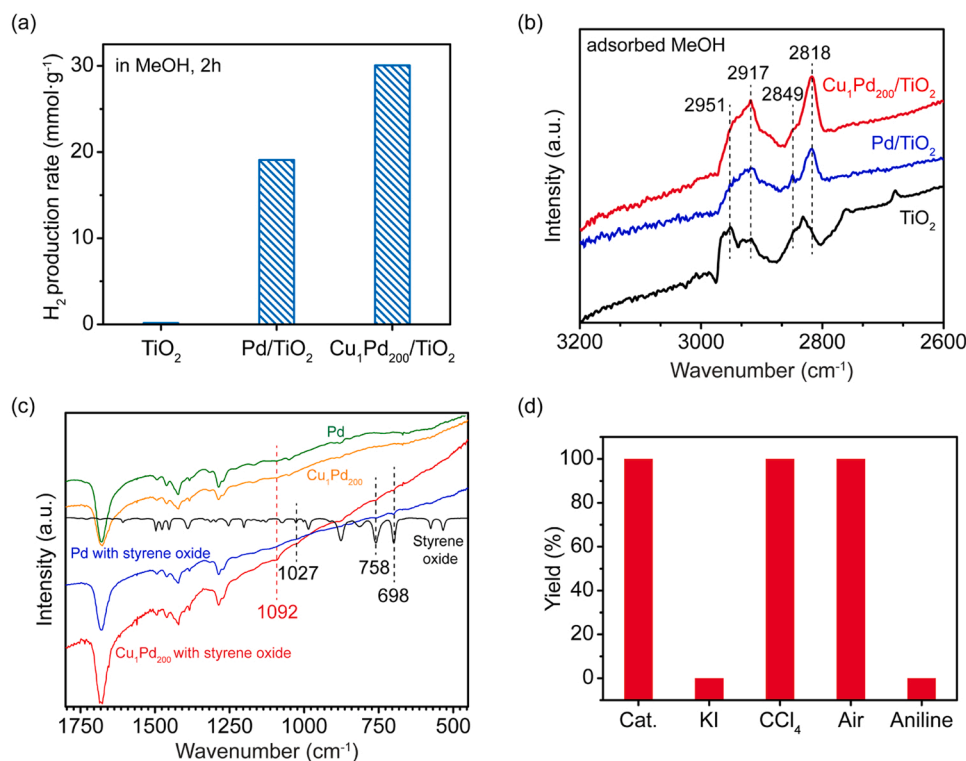
Fig. 5. (a) The photocatalytic hydrogen evolution performance of Cu_1Pd_{200}/TiO_2 and Pd/TiO_2, including bare TiO_2 for comparison. (b) The IR analysis of different photocatalyst samples (Cu_1Pd_{200}/TiO_2, Pd/TiO_2, and TiO_2) with methanol adsorption. (c) The IR profiles of Cu_1Pd_{200} and Pd nanosheets with styrene oxide adsorbed, including pure styrene oxide, clean Cu_1Pd_{200}, and Pd nanosheets as references. (d) The influence of various scavengers (1.0 mmol KI, CCl_4, air, and aniline) on photocatalytic alcoholysis of styrene oxide using Cu_1Pd_{200}/TiO_2 as the photocatalyst.

appears when the Cu_1Pd_{200} nanosheet has adsorbedstyrene oxide. This newly formed absorption band may originate from the weakened C-O bond after the complexation between Cu sites and O atoms [51]. The absorption frequency of 1092 cm^{-1} is also close to that of the chemisorption peak (at 1096 cm^{-1}) in the case of Cu_1Pd_{200} sample adsorbing ethanol, suggesting a similar complexation behavior via the C-O bond. This possible complexation could be realized when Cu dopant presents a lower electron density due to the partial electron transfer from Cu to Pd atoms. As expected, no unique absorption bands were observed in the case of Pd nanosheets. Therefore, the chemisorption of epoxides on Cu-doped photocatalyst can offer the effective activation of C-O bond from the three-member ring, further promoting the next ring-opening reaction. Additionally, the other IR absorption peaks (e.g., the intense one at 1679 cm^{-1}) are mainly ascribed to the characteristic absorption from PVP ligands on the surface based on the IR profiles in Fig. S14 (b). It should be pointed that no useful IR information can be extracted if the photocatalyst of Cu_1Pd_{200}/TiO_2 or Pd/TiO_2 is used to adsorb styrene oxide. Because the dominant signals come from the TiO_2 host instead of supported species in our cases as shown in Fig. S15.

To investigate the influence of surface metal sites on photocatalytic alcoholysis reaction, a series of control experiments have been performed by adding various scavengers during the reaction. As shown in Fig. 5(d), the presence of aniline can totally prohibit the alcoholysis, which can be ascribed to the occupation of Cu dopant and Ti cations through the strong coordination with -NH_2 group. Besides, the addition of oxalic acid can promote the reaction due to the activation of epoxides by protons as expected. More importantly, the hole scavenger (KI) can terminate the reaction quickly, indicating the vital role of holes for the generation of active methoxy species. In contrast, the electron scavenger (CCl_4) shows a minor influence, suggesting the fast reaction step between electrons and reactant during alcoholysis. This can also be verified by the control experiment performed in the air atmosphere, which displays the same photocatalytic activity as the case operated in the Ar atmosphere. Consequently, the activation of alcohols and epoxides on Cu dopant and the involvement of photo-generated holes from TiO_2 play key roles to achieve excellent photocatalytic performance in the

alcoholysis reaction of styrene oxide. The proposed reaction mechanism shown in Fig. 6 demonstrates the reaction paths. Firstly, methanol is dissociated on the TiO_2 surface to produce CH_3O_a. After light illumination, the holes and electrons could drive the formation of active methoxy species (e.g., methoxy radicals or anions). Meanwhile, another reactant of styrene oxide is chemisorbed on Cu dopant with a weakened C-O bond. Thus, the nucleophilic attack from active methoxy species to the complexed styrene oxide can be efficiently accomplished with a high yield of desired β-alkoxy alcohol product.

4. Conclusion

In summary, a ppm-level Cu dopant (39 ppm) based photocatalyst (Cu_1Pd_{200}/TiO_2) has been designed with Cu atoms highly dispersed on the surface of ultrathin Pd nanosheets (thickness of 2 nm). This is the first case of photocatalyst with a ppm-level loading of metal co-catalyst. Due to the presence of this ppm-level Cu dopant, a big difference in the photocatalytic performance of the alcoholysis reaction of epoxides has been made. The Cu-doped photocatalyst presents an ultra-high reaction rate of 176 mmol·g^{-1}·h^{-1} at room temperature under light illumination (100 mW·cm^2), which is 6 times and 17 times higher than Pd/TiO_2 with the absence of Cu element and bare TiO_2, respectively. This photocatalytic activity is nearly two orders of magnitude higher than that of the reported halide perovskite based photocatalyst. The incorporation of Cu dopant onto Pd nanosheets not only facilitates the generation of more active methoxy species, but also affords unique chemisorption of styrene oxide due to the electron transfer effect. Except for increasing the loading of co-catalyst metal as usual, this study provides another efficient strategy to enhance the ultimate photocatalytic activity. Briefly, we reconstruct the electronic structures of one metal substrate by doping with another metal species on the surface, which can dramatically reduce the loading of dopant metal down to a ppm level with the highly efficient atomic utilization.
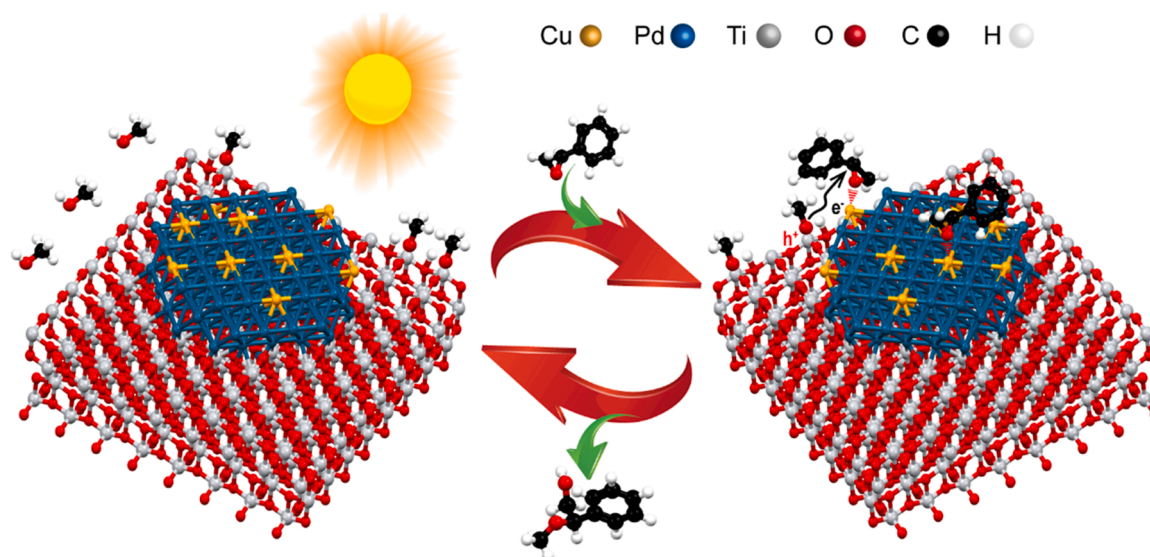
Fig. 6. The illustration of proposed photocatalytic reaction mechanisms, involving the activation of methanol on TiO_2 surface and styrene oxide on Cu dopant.

CRediT authorship contribution statement

Meilin Duan: Investigation. **Canyu Hu:** Investigation. **Delong Duan:** Investigation. **Ruitian Chen:** Investigation. **Chengming Wang:** Investigation. **Di Wu:** Investigation. **Tong Xia:** Investigation. **Hengjie Liu:** Investigation. **Yitao Dai:** Supervision, Writing – review & editing. **Ran Long:** Supervision, Writing – review & editing. **Li Song:** Investigation. **Yujie Xiong:** Supervision, Conceptualization, Writing – review & editing.

Declaration of Competing Interest

The authors declare that they have no known competing financial interests or personal relationships that could have appeared to influence the work reported in this paper.

Appendix A. Supporting information

Supplementary data associated with this article can be found in the online version at doi:10.1016/j.apcatb.2022.121211.

References

[1] A.S. Rao, S.K. Paknikar, J.G. Kirtane, Recent advances in the preparation and synthetic applications of oxiranes, Tetrahedron 39 (1983) 2323–2367.

[2] C. Baylon, G. Prestat, M.-P. Heck, C. Mioskowski, Synthesis of (−)-(4R,5R)-muricatacin using a regio- and stereospecific ring-opening of a vinyl epoxide, Tetrahedron Lett. 41 (2000) 3833–3835.

[3] G.H. Posner, J.P. Maxwell, M. Kahraman, Mild, fast, and stereoselective epoxide opening by ketone enolate anions. application to synthesis of the norlignan curculigine, J. Org. Chem. 68 (2003) 3049–3054.

[4] T. Weil, M. Kotke, C.M. Kleiner, P.R. Schreiner, Cooperative brønsted acid-type organocatalysis: alcoholysis of styrene oxides, Org. Lett. 10 (2008) 1513–1516.

[5] P. Dutta, P. Kalita, P.K. Baruah, Room temperature ring opening of epoxides over triflic acid functionalized cage like mesoporous materials, ChemistrySelect 1 (2016) 1650–1657.

[6] L. Zhang, C. Hu, W. Mei, J. Zhang, L. Cheng, N. Xue, W. Ding, J. Chen, W. Hou, Highly efficient sulfated Zr-doped titanoniobate nanoplates for the alcoholysis of styrene epoxide at room temperature, Appl. Surf. Sci. 357 (2015) 1951–1957.

[7] I. Sádaba, M. López Granados, A. Riisager, E. Taarning, Deactivation of solid catalysts in liquid media: the case of leaching of active sites in biomass conversion reactions, Green Chem. 17 (2015) 4133–4145.

[8] Y.-X. Zhou, Y.-Z. Chen, Y. Hu, G. Huang, S.-H. Yu, H.-L. Jiang, MIL-101-SO3H: a highly efficient brønsted acid catalyst for heterogeneous alcoholysis of epoxides under ambient conditions, Chem. Eur. J. 20 (2014) 14976–14980.

[9] Y.-X. Tan, X. Yang, B.-B. Li, D. Yuan, Rational design of a flu-type heterometallic cluster-based Zr-MOF, Chem. Commun. 52 (2016) 13671–13674.

[10] J.F. Blandez, A. Santiago-Portillo, S. Navalón, M. Giménez-Marqués, M. Álvaro, P. Horcajada, H. García, Influence of functionalization of terephthalate linker on the catalytic activity of UiO-66 for epoxide ring opening, J. Mol. Catal. A: Chem. 425 (2016) 332–339.

[11] S. Das, T. Asefa, Epoxide ring-opening reactions with mesoporous silica-supported Fe(III) catalysts, ACS Catal. 1 (2011) 502–510.

[12] N. Zhang, X. Li, H. Ye, S. Chen, H. Ju, D. Liu, Y. Lin, W. Ye, C. Wang, Q. Xu, J. Zhu, L. Song, J. Jiang, Y. Xiong, Oxide defect engineering enables to couple solar energy into oxygen activation, J. Am. Chem. Soc. 138 (2016) 8928–8935.

[13] Y. Dai, C. Li, Y. Shen, T. Lim, J. Xu, Y. Li, H. Niemantsverdriet, F. Besenbacher, N. Lock, R. Su, Light-tuned selective photosynthesis of azo- and azoxy-aromatics using graphitic C_3N_4, Nat. Commun. 9 (2018) 60.

[14] X. Lang, X. Chen, J. Zhao, Heterogeneous visible light photocatalysis for selective organic transformations, Chem. Soc. Rev. 43 (2014) 473–486.

[15] H. Li, C. Sun, M. Ali, F. Zhou, X. Zhang, D.R. MacFarlane, Sulfated carbon quantum dots as efficient visible-light switchable acid catalysts for room-temperature ring-opening reactions, Angew. Chem. Int. Ed. 54 (2015) 8420–8424.

[16] Y. Dai, H. Tüysüz, Lead-Free $Cs_3Bi_2Br_9$ perovskite as photocatalyst for ring-opening reactions of epoxides, ChemSusChem 12 (2019) 2587–2592.

[17] Y.-H. Liu, Q.-S. Liu, Z.-H. Zhang, Amberlyst-15 as a new and reusable catalyst for regioselective ring-opening reactions of epoxides to β-alkoxy alcohols, J. Mol. Catal. A: Chem. 296 (2008) 42–46.

[18] H.L. Tierney, A.E. Baber, J.R. Kitchin, E.C.H. Sykes, Hydrogen dissociation and spillover on individual isolated palladium atoms, Phys. Rev. Lett. 103 (2009), 246102.

[19] G. Kyriakou, M.B. Boucher, A.D. Jewell, E.A. Lewis, T.J. Lawton, A.E. Baber, H.L. Tierney, M. Flytzani-Stephanopoulos, E.C.H. Sykes, Isolated metal atom geometries as a strategy for selective heterogeneous hydrogenations, Science 335 (2012) 1209–1212.

[20] Q. Fu, Y. Luo, Catalytic activity of single transition-metal atom doped in Cu(111) surface for heterogeneous hydrogenation, J. Phys. Chem. C 117 (2013) 14618–14624.

[21] F.R. Lucci, J.L. Liu, M.D. Marcinkowski, M. Yang, L.F. Allard, M. Flytzani-Stephanopoulos, E.C.H. Sykes, Selective hydrogenation of 1,3-butadiene on platinum-copper alloys at the single-atom limit, Nat. Commun. 6 (2015) 8550.

[22] R. Long, Y. Li, Y. Liu, S. Chen, X. Zheng, C. Gao, C. He, N. Chen, Z. Qi, L. Song, J. Jiang, J. Zhu, Y. Xiong, Isolation of Cu atoms in Pd lattice: forming highly

selective sites for photocatalytic conversion of CO_2 to CH_4, J. Am. Chem. Soc. 139 (2017) 4486–4492.

[23] L. Liu, J. Li, Y. Ai, Y. Liu, J. Xiong, H. Wang, Y. Qiao, W. Liu, S. Tan, S. Feng, K. Wang, H. Sun, Q. Liang, A ppm level Rh-based composite as an ecofriendly catalyst for transfer hydrogenation of nitriles: triple guarantee of selectivity for primary amines, Green Chem. 21 (2019) 1390–1395.

[24] F. Zaccheria, F. Santoro, R. Psaro, N. Ravasio, CuO/SiO_2: a simple and efficient solid acid catalyst for epoxide ring opening, Green Chem. 13 (2011) 545–548.

[25] R. Su, R. Tiruvalam, A.J. Logsdail, Q. He, C.A. Downing, M.T. Jensen, N. Dimitratos, L. Kesavan, P.P. Wells, R. Bechstein, H.H. Jensen, S. Wendt, C.R. A. Catlow, C.J. Kiely, G.J. Hutchings, F. Besenbacher, Designer titania-supported Au-Pd nanoparticles for efficient photocatalytic hydrogen production, ACS Nano 8 (2014) 3490–3497.

[26] X. Han, Q. Kuang, M. Jin, Z. Xie, L. Zheng, Synthesis of titania nanosheets with a high percentage of exposed (001) facets and related photocatalytic properties, J. Am. Chem. Soc. 131 (2009) 3152–3153.

[27] Z. Zhang, Y. Liu, B. Chen, Y. Gong, L. Gu, Z. Fan, N. Yang, Z. Lai, Y. Chen, J. Wang, Y. Huang, M. Sindoro, W. Niu, B. Li, Y. Zong, Y. Yang, X. Huang, F. Huo, W. Huang, H. Zhang, Submonolayered Ru deposited on ultrathin Pd Nanosheets used for enhanced catalytic applications, Adv. Mater. 28 (2016) 10282–10286.

[28] Y. Li, Y. Yan, Y. Li, H. Zhang, D. Li, D. Yang, Size-controlled synthesis of Pd nanosheets for tunable plasmonic properties, CrystEngComm 17 (2015) 1833–1838.

[29] L. Zhang, F. Hou, Y. Tan, Shape-tailoring of CuPd nanocrystals for enhancement of electro-catalytic activity in oxygen reduction reaction, Chem. Commun. 48 (2012) 7152–7154.

[30] J. Tauc, R. Grigorovici, A. Vancu, Optical properties and electronic structure of amorphous germanium, Phys. Status Solidi B 15 (1966) 627–637.

[31] P. Edström, Examination of the revised Kubelka-Munk theory: considerations of modeling strategies, J. Opt. Soc. Am. A 24 (2007) 548–556.

[32] W.-K. Jo, S. Kumar, M.A. Isaacs, A.F. Lee, S. Karthikeyan, Cobalt promoted TiO_2/GO for the photocatalytic degradation of oxytetracycline and Congo Red, Appl. Catal., B 201 (2017) 159–168.

[33] X.Q. Huang, S.H. Tang, X.L. Mu, Y. Dai, G.X. Chen, Z.Y. Zhou, F.X. Ruan, Z.L. Yang, N.F. Zheng, Freestanding palladium nanosheets with plasmonic and catalytic properties, Nat. Nanotechnol. 6 (2011) 28–32.

[34] T. Ohba, H. Kubo, Y. Oshima, Y. Makita, N. Nakamura, H. Uehara, S. Takakusagi, K. Asakura, An origin for lattice expansion in PVP-protected small Pd metal nanoparticles, Bull. Chem. Soc. Jpn. 90 (2017) 720–727.

[35] M. Tang, W. Yuan, Y. Ou, G. Li, R. You, S. Li, H. Yang, Z. Zhang, Y. Wang, Recent progresses on structural reconstruction of nanosized metal catalysts via controlled-atmosphere transmission electron microscopy: a review, ACS Catal. 10 (2020) 14419–14450.

[36] W.Z. Tu, K. Chen, L.J. Zhu, H.C. Zai, E. Bin, X.X. Ke, C.F. Chen, M.L. Sui, Q. Chen, Y.J. Li, Tungsten-doping-induced surface reconstruction of porous ternary Pt-based alloy electrocatalyst for oxygen reduction, Adv. Funct. Mater. 29 (2019), 1807070.

[37] Y.W. Mu, Y. Han, J.L. Wang, J.G. Wan, G.H. Wang, Structures and magnetic properties of Pd-n clusters (n=3-19) doped by Mn atoms, Phys. Rev. A 84 (2011), 053201.

[38] V.R. Stamenkovic, B.S. Mun, K.J.J. Mayrhofer, P.N. Ross, N.M. Markovic, Effect of surface composition on electronic structure, stability, and electrocatalytic properties of Pt-transition metal alloys: Pt-skin versus Pt-skeleton surfaces, J. Am. Chem. Soc. 128 (2006) 8813–8819.

[39] J. Jung, S. Kang, L. Nicolai, J. Hong, J. Minar, I. Song, W. Kyung, S. Cho, B. Kim, J. D. Denlinger, F. Aires, E. Ehret, P.N. Ross, J. Shim, S. Nemsak, D. Noh, S. Han, C. Kim, B.S. Mun, Understanding the Role of Electronic Effects in CO on the Pt-Sn Alloy Surface via Band Structure Measurements, ACS Catal.

[40] K. Sasaki, H. Naohara, Y. Choi, Y. Cai, W.-F. Chen, P. Liu, R.R. Adzic, Highly stable Pt monolayer on PdAu nanoparticle electrocatalysts for the oxygen reduction reaction, Nat. Commun. 3 (2012) 1115.

[41] X. Yang, J. Xue, L. Feng, Pt nanoparticles anchored over Te nanorods as a novel and promising catalyst for methanol oxidation reaction, Chem. Commun. 55 (2019) 11247–11250.

[42] M. Wakisaka, S. Mitsui, Y. Hirose, K. Kawashima, H. Uchida, M. Watanabe, Electronic structures of Pt-Co and Pt-Ru alloys for CO-tolerant anode catalysts in polymer electrolyte fuel cells studied by EC-XPS, J. Phys. Chem. B 110 (2006) 23489–23496.

[43] D. Chen, P. Sun, H. Liu, J. Yang, Bimetallic Cu-Pd alloy multipods and their highly electrocatalytic performance for formic acid oxidation and oxygen reduction, J. Mater. Chem. A 5 (2017) 4421–4429.

[44] L.S. Kibis, A.I. Stadnichenko, S.V. Koscheev, V.I. Zaikoyskii, A.I. Boronin, Highly oxidized palladium nanoparticles comprising Pd^{4+} species: spectroscopic and structural aspects, thermal stability, and reactivity, J. Phys. Chem. C 116 (2012) 19342–19348.

[45] J.-K. Lee, H.-K. Rhee, Sulfur tolerance of zeolite beta-supported Pd-Pt catalysts for the isomerization of n-hexane, J. Catal. 177 (1998) 208–216.

[46] L. Ouyang, G.-J. Da, P.-F. Tian, T.-Y. Chen, G.-D. Liang, J. Xu, Y.-F. Han, Insight into active sites of Pd-Au/TiO_2 catalysts in hydrogen peroxide synthesis directly from H_2 and O_2, J. Catal. 311 (2014) 129–136.

[47] A.L. Cabrera, E. Morales, J.N. Armor, Kinetics of hydrogen desorption from palladium and ruthenium-palladium foils, J. Mater. Res. 10 (1995) 779–785.

[48] B. Jenewein, S. Penner, H. Gabasch, B. Klötzer, D. Wang, A. Knop-Gericke, R. Schlögl, K. Hayek, Hydride formation and stability on a Pd-SiO_2 thin-film model catalyst studied by TEM and SAED, J. Catal. 241 (2006) 155–161.

[49] H. Zhang, X. Yang, G. Gao, J. Yan, M. Zhao, H. Su, An efficient catalyst of CuPt/TiO_2 for photocatalytic direct dehydrogenation of methanol to methyl formate at ambient temperature, Catal. Sci. Technol. 12 (2022) 773–785.

[50] C. Fu, F. Li, J. Zhang, D. Li, K. Qian, Y. Liu, J. Tang, F. Fan, Q. Zhang, X.-Q. Gong, W. Huang, Site sensitivity of interfacial charge transfer and photocatalytic efficiency in photocatalysis: methanol oxidation on anatase $TiO2$ nanocrystals, Angew. Chem. Int. Ed. 60 (2021) 6160–6169.

[51] A.C. Lukaski, M.C.N. Enever, M.A. Barteau, Structure and reaction of oxametallacycles derived from styrene oxide on Ag(110), Surf. Sci. 601 (2007) 3372–3382.

[52] V. Arjunan, R. Anitha, L. Devi, S. Mohan, H. Yang, Comprehensive quantum chemical and spectroscopic (FTIR, FT-Raman, 1H, ^{13}C NMR) investigations of (1,2-epoxyethyl)benzene and (1,2-epoxy-2-phenyl)propane, Spectrochim. Acta, Part A 135 (2015) 120–136.